Tunnel junctions with multiferroic barriers

MARTIN GAJEK[1,2], MANUEL BIBES[3]*, STÉPHANE FUSIL[1], KARIM BOUZEHOUANE[1], JOSEP FONTCUBERTA[2], AGNÈS BARTHÉLÉMY[1] AND ALBERT FERT[1]

[1]Unité Mixte de Physique CNRS/Thales and Université Paris-Sud, Route départementale 128, 91767 Palaiseau, France
[2]Institut de Ciència de Materials de Barcelona, CSIC, Campus de la Universitat Autonoma de Barcelona, 08193 Bellaterra, Spain
[3]Institut d'Electronique Fondamentale, CNRS, Université Paris-Sud, 91405 Orsay, France
*e-mail: manuel.bibes@ief.u-psud.fr

Published online: 11 March 2007; doi:10.1038/nmat1860

Multiferroics are singular materials that can exhibit simultaneously electric and magnetic orders. Some are ferroelectric and ferromagnetic and provide the opportunity to encode information in electric polarization and magnetization to obtain four logic states. However, such materials are rare and schemes allowing a simple electrical readout of these states have not been demonstrated in the same device. Here, we show that films of $La_{0.1}Bi_{0.9}MnO_3$ (LBMO) are ferromagnetic and ferroelectric, and retain both ferroic properties down to a thickness of 2 nm. We have integrated such ultrathin multiferroic films as barriers in spin-filter-type tunnel junctions that exploit the magnetic and ferroelectric degrees of freedom of LBMO. Whereas ferromagnetism permits read operations reminiscent of magnetic random access memories (MRAM), the electrical switching evokes a ferroelectric RAM write operation. Significantly, our device does not require the destructive ferroelectric readout, and therefore represents an advance over the original four-state memory concept based on multiferroics.

The research on magnetic multilayers in the 1980s[1] has led to a new type of electronics exploiting the spin of the carriers, so-called spintronics[2]. Simultaneously, advances in ferroelectric thin-film research have produced technological applications in the sensor industry and consumer electronics[3]. Although magnetism and ferroelectricity usually exclude each other[4], it has been known since the 1960s that they can coexist in a few materials known as multiferroics[5,6]. These compounds exhibit magnetic and electric orders and thus provide a unique opportunity to exploit several functionalities in a single material[7,8].

A simple way to exploit this multifunctional character, which has never been reported yet, is to design magnetic tunnel junctions integrating a nanometric ferromagnetic–ferroelectric film as the tunnel barrier. The main problem is the scarcity of ferromagnetic–ferroelectric materials. Another key prerequisite is the stability of ferroelectricity at the very small thickness of a tunnel barrier[9].

Here, we report on the fabrication and characterization of epitaxial thin films of $La_{0.1}Bi_{0.9}MnO_3$ (LBMO). We show that these films are both ferromagnetic and ferroelectric and retain these properties down to a thickness of 2 nm. This allows us to use them as tunnel barriers in magnetic tunnel junctions and explore simultaneously two recently proposed concepts, namely spin-filtering by a ferromagnetic barrier[10–12] and the influence of ferroelectricity on the tunnelling properties[13–15]. Spin filters are tunnel junctions in which the tunnel barrier height is spin dependent because the bottom level of the conduction band in the ferromagnetic barrier material is spin-split by exchange. This allows the tunnelling electrons to be efficiently filtered according to their spin[12], in other words to create a highly spin-polarized current, thus leading to a large tunnel magnetoresistance (TMR) effect if one of the electrodes is also ferromagnetic[10,11] (see Fig. 1a). In addition, we observe an electroresistance (ER) effect that we suggest reflects a modulation of the tunnel current by the ferroelectric polarization in the LBMO barrier (see Fig. 1b). These junctions thus define a four-resistance-state system and constitute an important step towards the integration of nanometric multiferroic elements in spintronics devices.

The $BiMnO_3$ (BMO) perovskite has well-established ferromagnetic properties with a magnetic Curie temperature $T_{CM} = 105$ K (ref. 16) and a saturation magnetization of 3.6 μ_B/Mn (that is, ~540 e.m.u. cm^{-3}) (ref. 17). A ferroelectric character has been claimed by several groups. For example, Moreira dos Santos *et al.* have reported ferroelectric loops in bulk and polycrystalline thin-film samples, with a small polarization P of 0.15 μcm^{-2} (ref. 18). Kelvin force microscopy experiments[19] and electric-field-dependent second-harmonic generation signals[20] have also been used to infer a ferroelectric behaviour. The ferroelectric Curie point was reported to be $T_{CE} = 450$–490 K (refs 18,21). A hysteretic magnetic-field dependence of the dielectric constant of BMO ceramics was reported in ref. 22 and ascribed to the multiferroic character.

Practically, the stabilization of the pure BMO phase is difficult to achieve in bulk but is facilitated by partial substitution of Bi by isovalent La, with only little influence on the structural and magnetic properties at low La content[23] (T_{CM} is reduced to ~95 K for 10% La (ref. 23)). We have also found that the growth temperature–pressure window for obtaining optimal films is broader for La-substituted BMO films[24]. These reasons have led us to explore the multiferroic properties of LBMO and its potential for spintronics.

We have grown epitaxial LBMO films on $SrTiO_3$ (001) (STO) substrates and manganite $La_{2/3}Sr_{1/3}MnO_3$ (LSMO) buffers[25]. The LSMO layer can be used as a bottom metallic electrode for ferroelectric characterization and as a half-metallic ferromagnetic electrode[26] for spin-dependent tunnelling studies. X-ray diffraction analysis showed that 30-nm-thick LBMO films grow fully strained

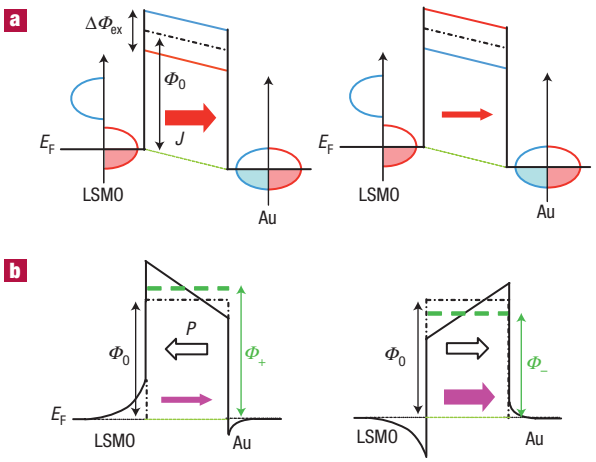

Figure 1 Schematic representation of the tunnel barrier potential profiles and tunnel currents for a ferromagnetic and a ferroelectric barrier. a, Schematic diagram of the spin-dependent tunnelling for parallel (left) or antiparallel (right) configurations of the LBMO and LSMO magnetizations, considering a half-metallic LSMO electrode with only spin-up states at the Fermi level E_F. For simplicity, we assume a non-ferroelectric LBMO barrier. Φ_0 is the barrier in the absence of ferromagnetism and $\Delta\Phi_{ex}$ is the exchange splitting. Spin-up is represented in red and spin-down in blue. In the parallel case, spin-up electrons tunnelling from LSMO experience a small barrier height ($\Phi_0 - \Delta\Phi_{ex}/2$), which results in a large current density (J, shown by a red arrow) and a low resistance. In the antiparallel case, these electrons tunnel through a larger barrier height ($\Phi_0 + \Delta\Phi_{ex}/2$), which results in a low current and a large resistance. **b**, Schematic diagram of the potential profile seen by the tunnelling electrons for the two directions of the barrier electric polarization, according to the model in ref. 13 (assuming a non-magnetic barrier). Φ_0 is the barrier in the absence of polarization. Φ_+ and Φ_- are the average barrier heights seen by the carriers when P points towards LSMO and Au, respectively. The black arrows indicate the direction of the ferroelectric polarization in the barrier. The purple arrows indicate the current density.

on the STO substrates. ϕ-scans carried out on several reflections of LBMO and STO indicate that the films are epitaxial and suggest that the LBMO has a tetragonal unit cell even though its space group may have a lower symmetry[25]. As shown in Fig. 2a,b, 30-nm-thick LBMO films exhibit a ferromagnetic behaviour with $T_{CM} \approx 90$ K, that is, close to the Curie temperature of bulk LBMO. The saturation magnetization is lower than that of bulk BMO, as often observed in BMO and LBMO films[27,28], and possibly due to Bi vacancies.

The ferroelectric nature of the LBMO films was characterized at room temperature using piezoresponse force microscopy (PFM) experiments. Figure 2c shows a PFM image collected after writing negatively or positively polarized stripes in a 30 nm LBMO film grown on LSMO. A clear contrast between up and down ferroelectric domains is observed. Contrast is also present in the non-written regions and we estimate the domain size to be about 50 nm. More quantitatively, the piezoelectric phase versus electric-field hysteresis cycle shown in Fig. 2d confirms that two remnant electric polarization states are stable in the film. The electric-field dependence of the piezoelectric coefficient d_{33} can be constructed by using the dependences of the phase and amplitude (not shown), see inset in Fig. 2d. The hysteresis cycle is not square as in thick ferroelectric capacitors[29], which is possibly due to the relatively small LBMO thickness, but it undoubtedly confirms the ferroelectric character. The d_{33} coefficient is rather small compared with the values found for lead zirconium titanate[30] or another Bi-based multiferroic material, $BiFeO_3$ ($d_{33} \approx 50$ pm V^{-1}) (ref. 31). Such a small value is not surprising in view of the small ferroelectric polarization found experimentally[18] or calculated[32] for $BiMnO_3$.

Given the similarities of bulk BMO and LBMO (ref. 23), it is anticipated that, as is thought to occur in BMO (refs 32,33), ferroelectricity in LBMO arises from the presence of directional 6s lone pairs on the Bi ions. Substrate-induced effects may not be essential but rather modify the magnitude of this off-centre distortion and thus possibly change T_{CE} and the polarization. The presence of a small fraction of La at the perovskite A site and the concomitant disorder in A-site occupancy could eventually modify the ordering temperature and the polarization as well. Further experimental and theoretical work is needed to better understand the ferroelectric properties of LBMO.

Figure 3 shows that the magnetic and ferroelectric properties of LBMO films are stable on thickness reduction down to a few nanometres. As can be seen in Fig. 3a, a 6-nm-thick film is still ferromagnetic, with roughly the same magnetization as a 30-nm-thick film (see Fig. 2a). Figure 3b shows that the temperature dependence of magnetization is also very similar to that of the 30 nm film (Fig. 2b), with a T_{CM} of around 90 K. These results stand in contrast with what is found for other ferromagnetic Mn oxides such as $La_{2/3}Ca_{1/3}MnO_3$ (LCMO) for which a strong reduction of M and T_{CM} is found when thickness decreases[34]. This is probably related to the type of ferromagnetic interaction active in LBMO, super-exchange, which is not carrier mediated and is thus insensitive to charge localization effects that tend to occur at reduced dimensions in double-exchange systems such as LCMO or LSMO. We emphasize that ferromagnetism is retained down to even lower LBMO thickness (2 nm), as demonstrated by the observation of a spin-filter effect in LSMO/LBMO(2 nm)/Au tunnel junctions, see later.

Figure 3c–e shows PFM images of a 2 nm (that is, 5 unit cells) LBMO film grown on LSMO. Figure 3c was collected after writing 1.5-μm-wide stripes at a voltage of ±2 V. A clear contrast is observed between the two opposite polarities. To demonstrate the switchable character of this contrast, a 1 μm^2 square was written with a positive voltage (2 V) onto a negatively polarized stripe (Fig. 3d) and vice versa (Fig. 3e). Clearly, the PFM contrast is reversed, which shows that polarization in this film is indeed switchable. We have checked that this contrast was stable over several hours. Control experiments were carried out on samples with non-ferroelectric layers such as STO(8 nm)/LSMO/STO and no contrast was observed. The good stability of the contrast observed in the case of LBMO supports the well-preserved ferroelectric nature of LBMO films as thin as 2 nm. To be more quantitative on the thickness dependence of ferroelectricity in LBMO films is difficult, as the signal measured on very thin films was too low to estimate the d_{33} coefficient. The degradation of ferroelectricity at low thickness is a long-standing issue that has attracted the attention of both theorists[35] and experimentalists[36,37]. We anticipate that the presumably small value of the LBMO polarization strongly limits depolarizing field effects, hence enabling films to retain a ferroelectric character at room temperature even at a thickness of 2 nm (or maybe even less), contrary to what occurs in some systems with a stronger polarization[35]. We further note that even though we did not attempt to measure the ferroelectric Curie temperature of our LBMO films, the observation of a ferroelectric character at 300 K sets a lower limit for T_{CE}.

To exploit the multiferroic character of LBMO in spintronics, we have integrated such ultrathin ferromagnetic–ferroelectric LBMO films as barriers in tunnel junctions (40 ± 10 nm in diameter) using an LSMO film (30 nm) as the bottom electrode and a gold layer for the top one (for lithography details, see ref. 38

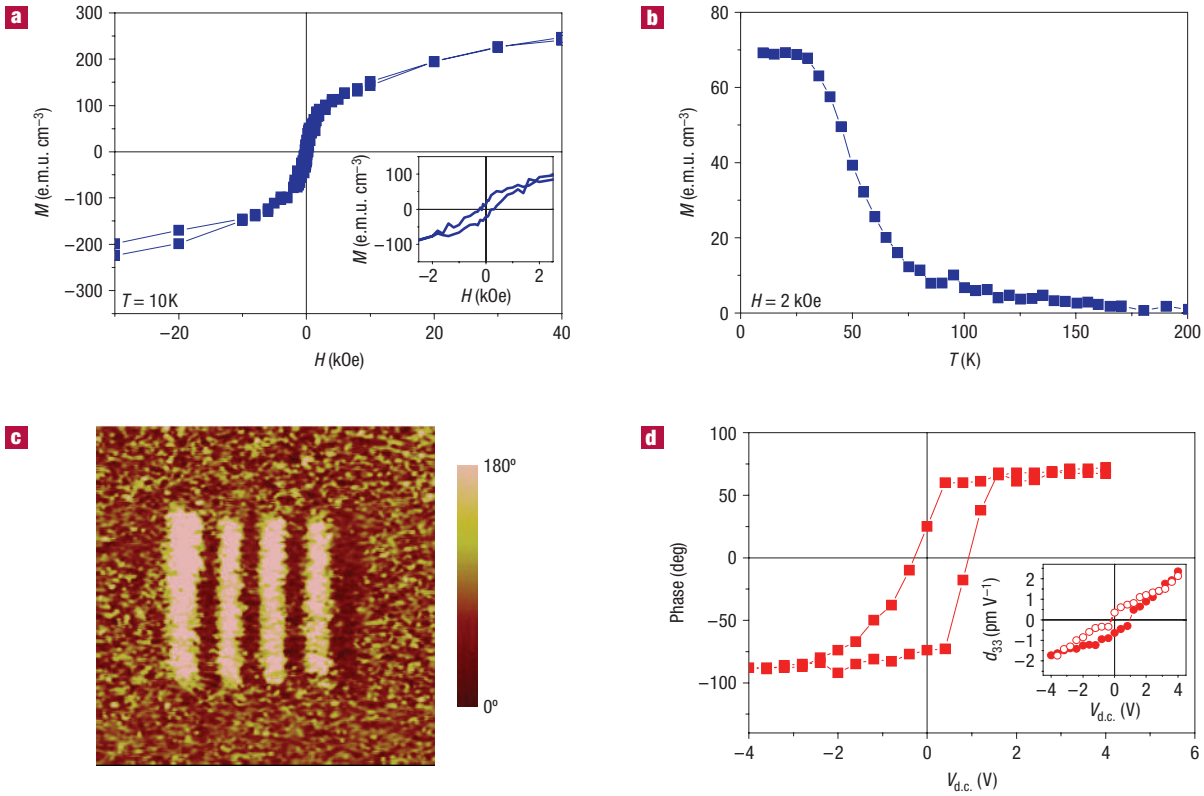

Figure 2 Magnetic and ferroelectric properties of 30 nm LBMO films. a,**b**, Field (**a**) and temperature (**b**) dependence of the magnetization of a 30 nm LBMO film. **c**, PFM phase image after applying a positive (4 V) or negative (−4 V) writing voltage along stripes on a 30 nm LBMO film grown on an LSMO electrode. **d**, Variation of the piezoresponse phase with the applied voltage.

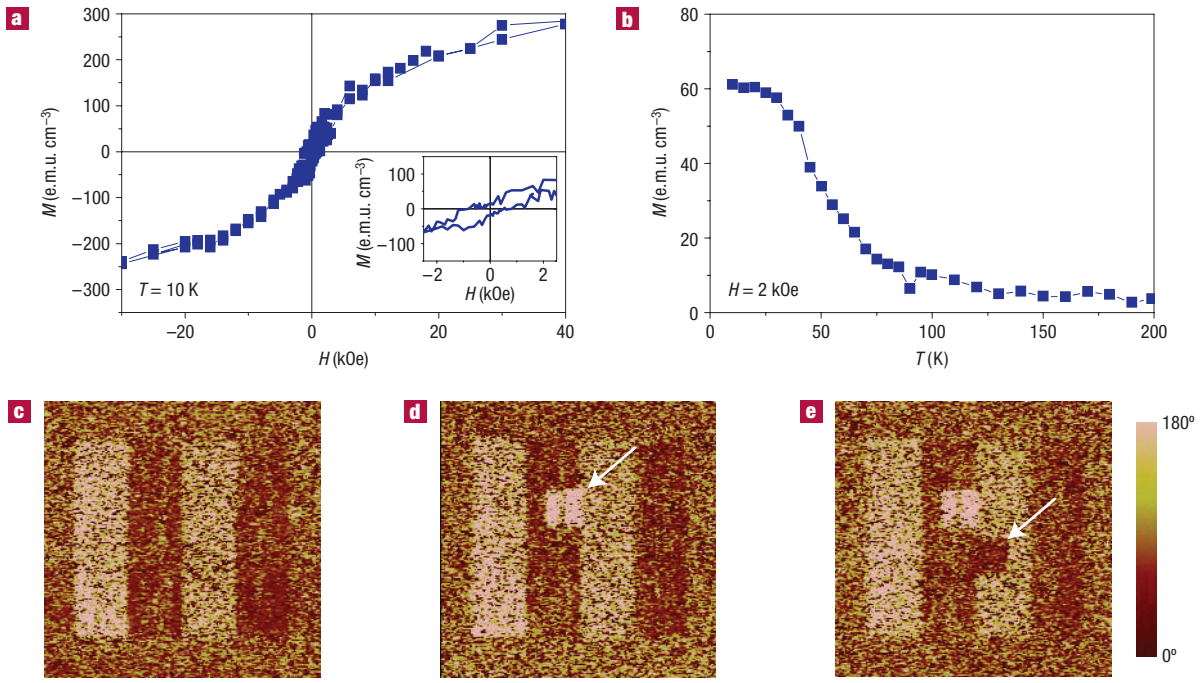

Figure 3 Magnetic and ferroelectric properties of ultrathin LBMO films. a,**b**, Field (**a**) and temperature (**b**) dependence of the magnetization of a 6 nm LBMO film. **a** is reused with permission from ref. 39. Copyright 2006, American Institute of Physics. **c**–**e**, PFM phase images of a 2 nm LBMO film grown on an LSMO electrode, after writing first four voltage stripes (**c**) and then two 1 μm^2 squares at opposite voltage (**d**,**e**).

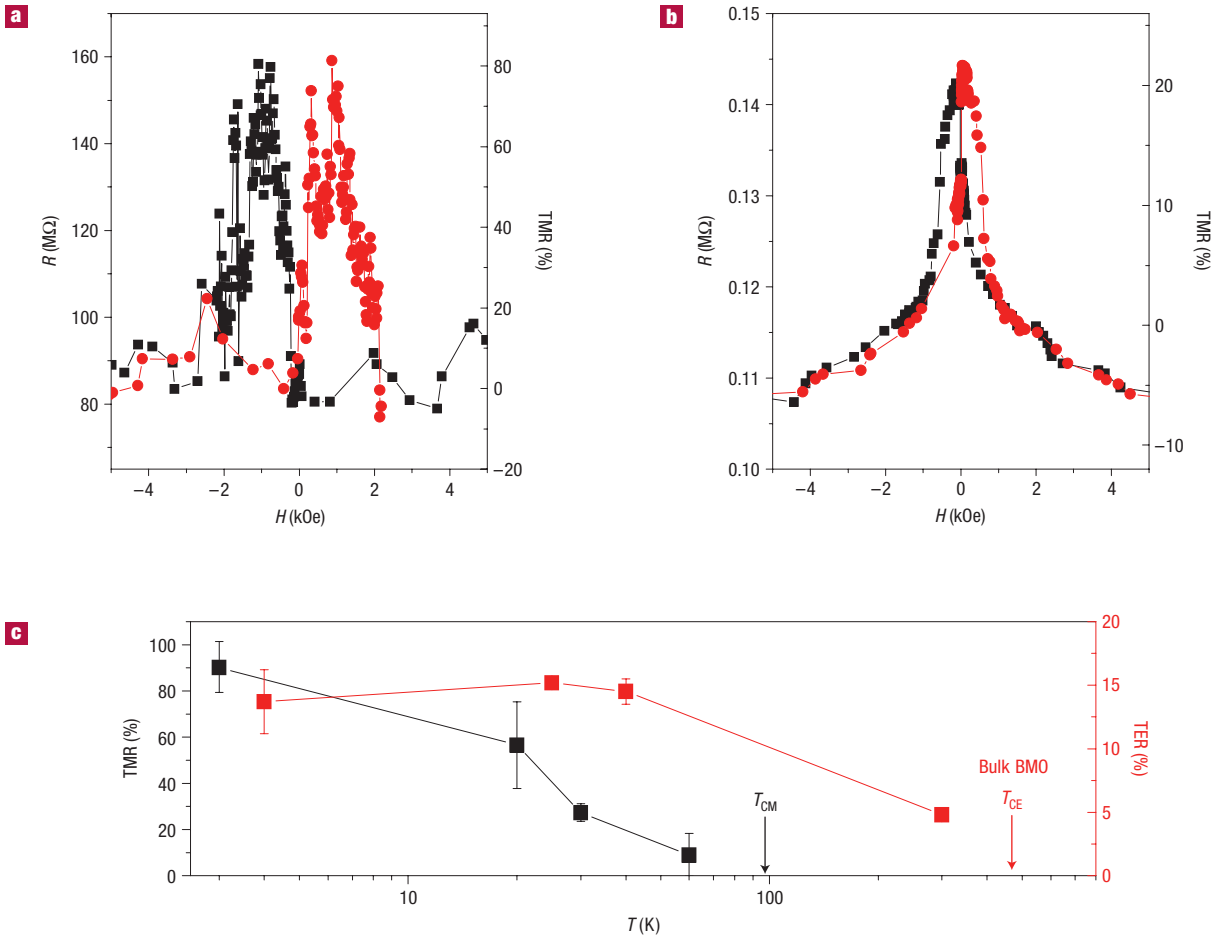

Figure 4 Tunnel magnetoresistance of LBMO-based spin-filters and temperature dependence of the tunnel magnetoresistance and electroresistance. a,**b**, Tunnel magnetoresistance curves at 4 K at $V_{d.c.} = 10$ mV in an LSMO/STO(1.6 nm)/LBMO(4 nm)/Au junction (**a**) and an LSMO/LBMO(2 nm)/Au junction (**b**). Negative to positive: red; positive to negative: black. **c**, Temperature dependence of the TMR of an LSMO/STO(1.6 nm)/LBMO(4 nm)/Au junction and of the tunnel electroresistance (TER) of an LSMO/LBMO(2 nm)/Au junction. The arrows indicate the ferromagnetic Curie temperature measured on LBMO films (see Figs 2b and 3b) and the ferroelectric Curie temperature reported for bulk BMO (see text).

and the Methods section). An ultrathin (a few unit cells) STO spacer was intercalated between the two magnetic layers in some of the samples. This proved to be an efficient way to decrease the ferromagnetic coupling existing between adjacent LBMO and LSMO layers and thus achieve independent magnetization reversals[25]. As shown in Fig. 4a, junctions integrating this STO spacer exhibit a TMR effect (defined as the difference between the junction resistance in the antiparallel, ap, and parallel, p, configurations of the LSMO and LBMO magnetizations, that is, $\mathrm{TMR} = (R_{ap} - R_p)/R_p$) with two well-defined switching fields, even though a fully antiparallel alignment is not achieved because of the low remanence of LBMO. This suggests a ferromagnetic domain size smaller than the junction area, ~2,000 nm^2. For an LBMO thickness of 4 nm, a large TMR is obtained at 3 K at 10 mV (81% in the curve shown in Fig. 4a and up to 90%, see ref. 39). This TMR effect is due to the spin-filtering effect[11,12] by the ferromagnetic LBMO barrier. Taking a value of 90% for the spin polarization of the LSMO/STO interface, a maximum spin-filtering efficiency (SFE) of 35% is inferred[40]. We note that the positive sign of the SFE is in agreement with what is expected from the calculated band structure of $BiMnO_3$ (ref. 32), that is, a lower barrier height for spin-up than for spin-down. We point out that the SFE and hence the TMR should be much larger if a better-defined ap state could be achieved. The influence of a ferromagnetic coupling between adjacent LBMO and LSMO layers is evident from TMR curves collected on junctions without an STO spacer: in this case the switching fields are poorly defined (see Fig. 4b). In the absence of such a spacer and at lower LBMO thickness (2 nm), the junction resistance and the maximum TMR are lower (22% in the example in Fig. 4b). As can be seen in Fig. 4c (black squares), the TMR decreases with temperature and vanishes at about 60 K, that is, lower than the T_{CM} found for a 6 nm film (Fig. 3b). However, because finite-size effects become increasingly important as thickness decreases, it is possible that the T_{CM} of 2–4-nm-thick films is significantly reduced from the bulk value. Nevertheless, the observation of a spin-filtering effect by such thin LBMO layers demonstrates their ferromagnetic character. We therefore conclude that our LBMO films are thus both ferromagnetic and ferroelectric, that is, multiferroic, down to 2 nm.

Just as the ferromagnetic nature of the LBMO barrier affects the tunnel current and produces a spin-filter effect, its ferroelectric nature is also expected to influence the tunnelling properties. The influence of the electrical polarization on tunnelling has been investigated from both experimental[41] and theoretical[13,14]

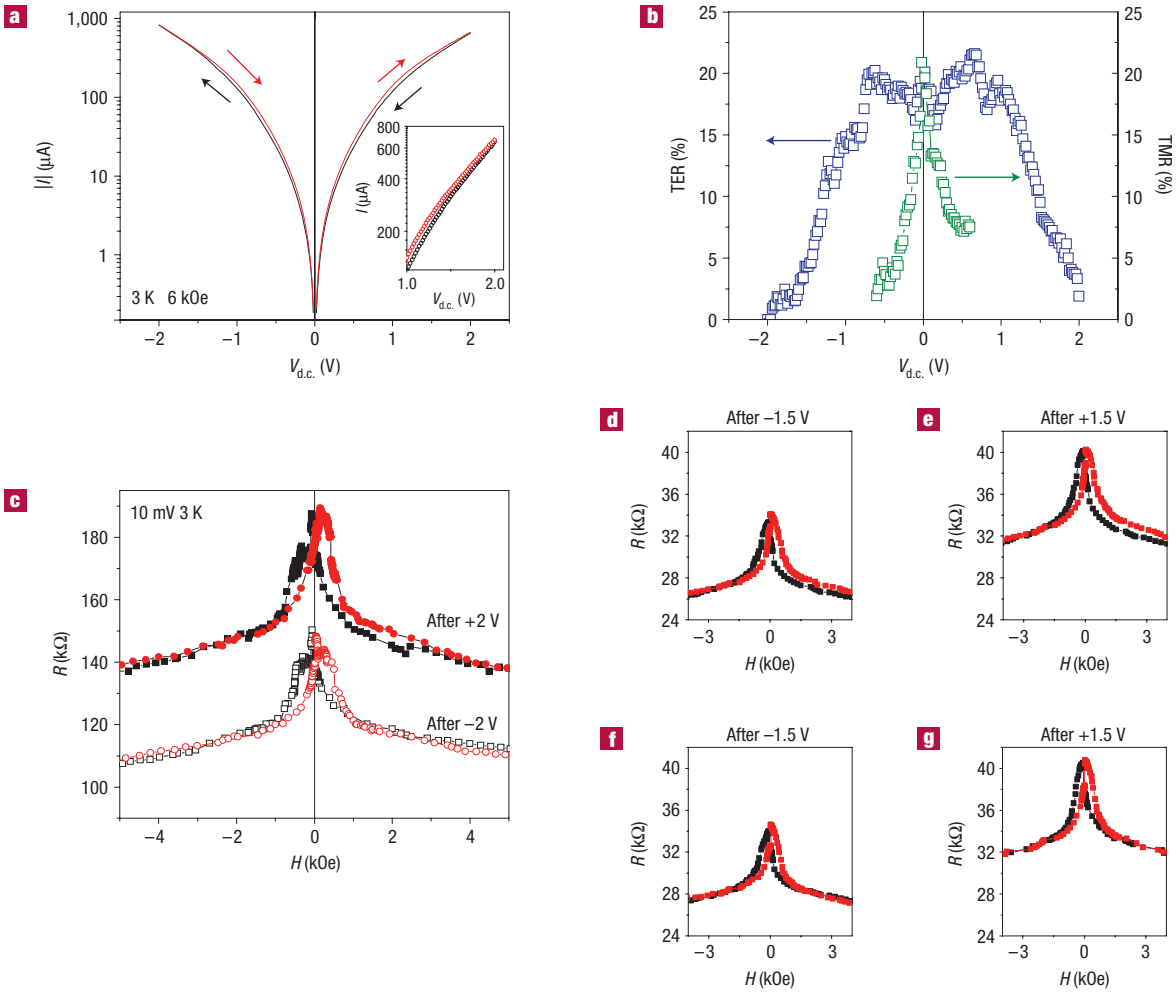

Figure 5 Tunnel electroresistance and its combination with tunnel magnetoresistance in LBMO-based spin filters, defining a four-resistance-state system. **a**, Bias-voltage dependence of the current of an LSMO/LBMO(2 nm)/Au tunnel junction, for two different bias sweep directions (negative to positive: red; positive to negative: black). Inset: $I(V)$ curves up to the maximum applied bias voltage of 2 V. **b**, Bias dependence of the tunnel electroresistance and tunnel magnetoresistance measured on an LSMO/LBMO(2 nm)/Au junction. **c**, Tunnel magnetoresistance curves at 4 K at $V_{d.c.} = 10$ mV in an LSMO/LBMO(2 nm)/Au junction, after applying a voltage of +2 V (filled symbols) and −2 V (open symbols). The combination of the electroresistance effect and the tunnel magnetoresistance produces a four-resistance-state system. **d–g**, Tunnel magnetoresistance curves at 4 K at $V_{d.c.} = 10$ mV in another LSMO/LBMO(2 nm)/Au junction on the same sample, after applying a large positive or negative voltage.

points of view. A first mechanism leading to a modulation of the tunnel current by the polarization of the barrier is the variation of the barrier thickness owing to the converse piezoelectric effect. This mechanism gives rise to asymmetrical current–voltage, $I(V)$, curves with a shift of the conductance minimum to a non-zero voltage[14]. From the low d_{33} value estimated by PFM (see Fig. 2d), we expect a shift of only 3.6 mV. A second mechanism for the influence of the ferroelectric polarization is related to the charge screening at the electrode–barrier interfaces and the difference in its spatial extension at both sides of the barrier. This screening controls the depolarizing field across the junction and therefore the profile of the barrier potential seen by the tunnelling electrons[13] (see Fig. 1b). By using electrodes with different screening lengths, the average barrier height is different for different orientations of the polarization. In our case, the electrodes are Au and LSMO for which screening lengths of 0.07 nm and 0.2–1.9 nm (refs 42,43), respectively, have been reported. This second mechanism is thus likely to be active in our LBMO-based junctions.

In Fig. 5a, we show $I(V)$ curves obtained at 6 kOe by cycling the bias voltage between +2 and −2 V in a LSMO/LBMO(2 nm)/Au junction. A noticeable hysteresis is observed: the tunnelling current is smaller (larger) for a given voltage when the voltage is swept from +2 V to −2 V (from −2 V to +2 V). A similar hysteresis is observed at low magnetic field, in the ap state, and for different junctions (see the Supplementary Information). We also note that the voltage dependence of the current and the conductance $G = \mathrm{d}I/\mathrm{d}V$ is the one that is expected if transport occurs by direct tunnelling (see the Supplementary Information). The hysteresis in the $I(V)$ curves corresponds to an ER effect that we define as the normalized difference between the $I(V)$ curves at increasing and decreasing voltage $\mathrm{ER} = [I(V < 0 \rightarrow V > 0) - I(V > 0 \rightarrow V < 0)]/I(V > 0 \rightarrow V < 0)$. The ER has been observed for different values of the magnetic field and in several junctions. It is reproducible and does not depend on the voltage sweep rate (see the Supplementary Information). As shown in Fig. 5b, the ER amounts to 22% and we can distinguish a low-voltage regime where the ER is roughly constant, and a symmetric high-voltage regime where the

ER decreases to zero. This may reflect a transition from tunnelling through to over the tunnel barrier.

Significantly, the ER is largest at low voltage, as is also the case for TMR (which decreases with voltage, presumably owing to the excitation of magnons in the magnetic barrier[11,44] and to density-of-state effects[45]). Consequently, it is possible to combine both ER and TMR to obtain four different resistance states at low bias voltage. This is illustrated by Fig. 5c, which shows two TMR curves recorded at 10 mV after applying a large positive or negative voltage (+2 V or −2 V) across the junction. We note that this effect has been observed in several junctions and that it is possible to cycle between the different states via the application of a magnetic and/or electric field (see Fig. 5d–g). Our junctions based on a multiferroic tunnel barrier therefore define a four-resistance-state system.

Several mechanisms have been invoked to explain electroresistance effects in oxides[46] (Mott insulator–metal transition, charging/discharging trap states[47], formation of local current domains[48], electronic modifications at dislocations[49]). These effects are usually very large (orders of magnitude in variation) and the switching is sharp. In addition, they have been observed for much thicker oxide layers (>30 nm), far beyond the limit for tunnelling. This contrasts with our observation of a smooth electroresistance of ∼20% in junctions with a 2-nm-thick barrier through which current flows by tunnelling (our $G(V)$ curves can be well-fitted by a parabolic function beyond the magnon excitation regime, that is, ±150 mV). We have also checked that $I(V)$ curves up to ±2 V measured on LSMO/STO/Au junctions fabricated by the same technique do not show hysteresis. We therefore suggest that the observed electroresistance effects most likely arise from ferroelectric switching in the LBMO tunnel barrier. A possible mechanism is the one proposed by Zhuravlev *et al.*[13] that considers the asymmetric deformation of the barrier potential profile induced by the ferroelectric polarization of LBMO. If we assume that the $P(E)$ loop of the ferroelectric barrier is hard to saturate (as can be inferred from the d_{33} versus E dependence of a 30 nm LBMO film, see inset of Fig. 2d), we do not expect to observe sharp switching events in the $I(V)$ curves, in agreement with the experimental data. The observation of an increase of the ER with increasing the maximum applied voltage (not shown) is also consistent with this picture. Significantly, the ER decreases with temperature but is still ∼4% at room temperature (see Fig. 4c). This is consistent with the observation of a ferroelectric character at 300 K (see Fig. 3c–e) and is reasonable in view of the reported values of $T_{CE} \approx 450$–500 K for bulk BMO, see refs 18,21 (the T_{CE} of bulk LBMO is not known at present). All of these arguments support our interpretation of hysteretic $I(V)$ curves and the ER effect on the basis of the ferroelectric character of the LBMO barrier.

In summary, we have reported the concomitant observation of ferromagnetism and ferroelectricity in epitaxial thin films. The material we have chosen is $La_{0.1}Bi_{0.9}MnO_3$ and, remarkably, it retains its multiferroic character in thin-film form down to a thickness of 2 nm. Using such ultrathin LBMO layers as tunnel barriers allows the device to operate as a four-resistance-state system. Consequently, our results suggest that it is possible to encode quaternary information by both ferromagnetic and ferroelectric order parameters, and to read it non-destructively by a resistance measurement. We anticipate our results to be a starting point for more studies on the interplay between ferroelectricity and spin-dependent tunnelling, and for the use of nanometric multiferroic elements in prototype devices. On a wider perspective, they may open the way towards novel reconfigurable logic spintronics architectures and to electrically controlled readout in quantum-computing schemes using the spin-filter effect[50].

METHODS

The LBMO films used in this study were grown by pulsed laser deposition on $SrTiO_3(001)$ single-crystalline substrates using a KrF laser ($\lambda = 248$ nm) with a fluence of 2 J cm^{-2} and a repetition rate of 2 Hz. The oxygen partial pressure was set to 0.1 mbar and the substrate temperature to 625 °C. LSMO templates were grown *in situ* before LBMO deposition (at a pressure of 0.2 mbar and a temperature of 700 °C) except for tunnel-junction structures for which the LSMO and LSMO/STO templates were grown previously by pulsed laser deposition on STO substrates with a Nd:YAG laser (at a frequency of 2.5 Hz, a pressure of 0.41 mbar and a temperature of 720 °C). After growing the LBMO, the samples were cooled to room temperature in 1 bar of pure oxygen. Tunnel junctions 40 ± 10 nm in diameter were defined by spinning a thin (∼30 nm) photoresist layer on the LSMO/LBMO or LSMO/STO/LBMO bilayers and indenting it with a conductive-tip atomic force microscope (AFM) while monitoring the LSMO-tip resistance in real time (see ref. 38 for details). The indents where subsequently filled with ∼100 nm of Au. Magnetization was measured in a Quantum Design superconducting quantum interference device with the magnetic field applied in the plane. PFM was carried out with a Digital Instruments Nanoscope IV AFM with CrPt-coated conducting tips. PFM signals were extracted through the AFM signal access module to an SR830 lock-in amplifier. The phase and amplitude of the signal were collected simultaneously. The a.c. modulation voltage applied between the tip and the bottom electrode for reading had a typical frequency of 4 kHz and a peak-to-peak amplitude of 0.5 V. The junction transport properties were measured using a Keithley 6514 electrometer and a Keithley K230 voltage source or a Keithley 2400 multimeter, in an Oxford Instruments cryostat (3–300 K) equipped with an electromagnet (0–6 kOe). Positive voltage corresponded to electrons tunnelling from the bottom electrode to the top electrode.

Received 21 November 2006; accepted 29 January 2007; published 11 March 2007.

References

1. Baibich, M. N. *et al.* Giant magnetoresistance of (001)Fe/(001)Cr magnetic superlattices. *Phys. Rev. Lett.* **61**, 2472–2475 (1988).
2. Zutic, I., Fabian, J. & Das Sarma, S. Spintronics: Fundamentals and applications. *Rev. Mod. Phys.* **76**, 323–410 (2004).
3. Scott, J. F. *Ferroelectric Memories* (Springer, Berlin, 2000).
4. Hill, N. A. Why are there so few magnetic ferroelectrics? *J. Phys. Chem. B* **104**, 6694–6709 (2000).
5. Smolenskii, G. A. & Chupis, I. E. Ferroelectromagnets. *Sov. Phys. Usp.* **25**, 475–493 (1982).
6. Eerenstein, W., Mathur, N. D. & Scott, J. F. Multiferroic and magnetoelectric materials. *Nature* **442**, 759–765 (2006).
7. Hur, N. *et al.* Electric polarization reversal in a multiferroic material induced by magnetic fields. *Nature* **429**, 392–395 (2004).
8. Kimura, T. *et al.* Magnetic control of ferroelectric polarization. *Nature* **426**, 55–58 (2003).
9. Ahn, C. H., Rabe, K. M. & Triscone, J.-M. Ferroelectricity at the nanoscale: local polarization in oxide thin films and heterostructures. *Science* **303**, 488–491 (2004).
10. LeClair, P. *et al.* Large magnetoresistance using hybrid spin filter devices. *Appl. Phys. Lett.* **80**, 625–627 (2003).
11. Gajek, M. *et al.* Spin filtering through ferromagnetic $BiMnO_3$ tunnel barriers. *Phys. Rev. B* **72**, 020406(R) (2005).
12. Moodera, J. S., Hao, X., Gibson, G. A. & Meservey, R. Electron-spin polarization in tunnel junctions in zero applied field with ferromagnetic EuS barriers. *Phys. Rev. Lett.* **61**, 637–640 (1988).
13. Zhuravlev, M. Y., Sbirianov, R. F., Jaswal, S. S. & Tsymbal, E. Y. Giant electroresistance in ferroelectric tunnel junctions. *Phys. Rev. Lett.* **94**, 246802 (2005).
14. Kohlstedt, H., Pertsev, N. A., Rodriguez-Contreras, J. & Waser, R. Theoretical current-voltage characteristics of ferroelectric tunnel junctions. *Phys. Rev. B* **72**, 125341 (2005).
15. Tsymbal, E. Y. & Kohlstedt, H. Tunneling across a ferroelectric. *Science* **313**, 181–183 (2006).
16. Sugawara, F., Iida, S., Syono, Y. & Akimoto, S. New magnetic perovskites $BiMnO_3$ and $BiCrO_3$. *J. Phys. Soc. Jpn.* **20**, 1529 (1965).
17. Chiba, H., Atou, T. & Syono, Y. Magnetic and electric properties of $Bi_{1-x}Sr_xMnO_3$: Hole-doping effect on ferromagnetic perovskite $BiMnO_3$. *J. Solid State Chem.* **132**, 139–143 (1997).
18. Moreira dos Santos, A. *et al.* Evidence for the likely occurrence of magnetoferroelectricity in the simple perovskite $BiMnO_3$. *Solid State Commun.* **122**, 49–52 (2002).
19. Son, J. Y., Kim, B. G., Kim, C. H. & Cho, J. H. Writing polarization bits on the multiferroic $BiMnO_3$ thin film using Kelvin probe force microscope. *Appl. Phys. Lett.* **84**, 4971–4973 (2004).
20. Sharan, A. *et al.* Bismuth manganite: A multiferroic with a large nonlinear optical signal. *Phys. Rev. B* **69**, 214109 (2004).
21. Chi, Z. H. *et al.* Manifestation of ferroelectromagnetism in multiferroic $BiMnO_3$. *J. Appl. Phys.* **98**, 103519 (2005).
22. Kimura, T. *et al.* Magnetocapacitance effect in multiferroic $BiMnO_3$. *Phys. Rev. B* **67**, 180401(R) (2003).
23. Troyanchuk, I. O., Mantyskaja, O. S., Szymczak, H. & Shvedun, M. Y. Magnetic phase transition in the system $La_{1-x}Bi_xMnO_{3+\lambda}$. *Low Temp. Phys.* **28**, 569–573 (2002).
24. Gajek, M. *Filtrage de spin par des barrières multiferroïques*, Thesis (Université Paris VI, April 2006).
25. Gajek, M., Bibes, M., Barthélémy, A., Varela, M. & Fontcuberta, J. Perovskite-based heterostructures integrating ferromagnetic-insulating $La_{0.1}Bi_{0.9}MnO_3$. *J. Appl. Phys.* **97**, 103909 (2005).
26. Bowen, M. *et al.* Nearly total spin-polarization in $La_{2/3}Sr_{1/3}MnO_3$ from tunneling experiments. *Appl. Phys. Lett.* **82**, 233–235 (2003).
27. Ohshima, E., Saya, Y., Nantoh, M. & Kawai, M. Synthesis and magnetic property of the perovskite $Bi_{1-x}Sr_xMnO_3$ thin film. *Solid State Commun.* **116**, 73–76 (2000).

28. Eerenstein, W., Morrison, F. D., Scott, J. F. & Mathur, N. D. Growth of highly resistive $BiMnO_3$ films. *Appl. Phys. Lett.* **87**, 101906 (2005).
29. Dawber, M., Rabe, K. M. & Scott, J. F. Physics of thin-film ferroelectric oxides. *Rev. Mod. Phys.* **77**, 1083–1130 (2005).
30. Nagarajan, V. *et al.* Dynamics of ferroelastic domains in ferroelectric thin films. *Nature Mater.* **2**, 43–47 (2003).
31. Yang, S. Y. *et al.* Metalorganic chemical vapor deposition of lead-free ferroelectric $BiFeO_3$ films for memory applications. *Appl. Phys. Lett.* **87**, 102903 (2005).
32. Shishidou, T., Mikamo, N., Uratani, Y., Ishii, F. & Oguchi, T. First-principles study on the electronic structure of bismuth transition-metal oxides. *J. Phys. Condens. Matter* **16**, S5677–S5683 (2004).
33. Seshadri, R. & Hill, N. A. Visualizing the role of Bi 6s "lone pairs" in the off-center distortion in ferromagnetic $BiMnO_3$. *Chem. Mater.* **13**, 2892–2899 (2001).
34. Bibes, M. *et al.* Nanoscale multiphase separation at $La_{2/3}Ca_{1/3}MnO_3/SrTiO_3$ interfaces. *Phys. Rev. Lett.* **87**, 067210 (2001).
35. Junquera, J. & Ghosez, P. Critical thickness for ferroelectricity in perovskite ultrathin films. *Nature* **422**, 506–509 (2003).
36. Lichtensteiger, C., Triscone, J.-M., Junquera, J. & Ghosez, P. Ferroelectricity and tetragonality in ultrathin $PbTiO_3$ films. *Phys. Rev. Lett.* **94**, 047603 (2005).
37. Fong, D. D. *et al.* Ferroelectricity in ultrathin perovskite films. *Science* **304**, 1650–1653 (2004).
38. Bouzehouane, K. *et al.* Nanolithography based on real-time electrically controlled indentation with an atomic force microscope for nanocontact elaboration. *Nano Lett.* **3**, 1599–1602 (2003).
39. Gajek, M. *et al.* $La_{2/3}Sr_{1/3}MnO_3$–$La_{0.1}Bi_{0.9}MnO_3$ heterostructures for spin filtering. *J. Appl. Phys.* **99**, 08E504 (2006).
40. Jullière, M. Tunneling between ferromagnetic films. *Phys. Lett. A* **54**, 225–226 (1975).
41. Rodriguez Contreras, J. *et al.* Resistive switching in metal-ferroelectric-metal junctions. *Appl. Phys. Lett.* **83**, 4595–4597 (2003).
42. Hong, X., Posadas, A. & Ahn, C. H. Examining the screening limit of field effect devices via the metal-insulator transition. *Appl. Phys. Lett.* **86**, 142501 (2005).
43. Dzero, M., Gor'kov, L. P. & Kresin, V. Z. On magnetoconductivity of metallic manganite phases and heterostructure. *Int. J. Mod. Phys. B* **17**, 2095–2115 (2003).
44. Tsui, D. C., Dietz, R. E. & Walker, L. R. Multiple magnon excitation in NiO by electron tunneling. *Phys. Rev. Lett.* **27**, 1729–1732 (1971).
45. Bowen, M. *et al.* Spin-polarized tunneling spectroscopy in tunnel junctions with half-metallic electrodes. *Phys. Rev. Lett.* **95**, 137203 (2005).
46. Oligschlaeger, R., Waser, R., Meyer, R., Karthäuser, S. & Dittman, R. Resistive switching and data reliablility of epitaxial $(Ba,Sr)TiO_3$ thin films. *Appl. Phys. Lett.* **88**, 042901 (2006).
47. Watanabe, Y. *et al.* Current-driven insulator-conductor transition and nonvolatile memory in chromium-doped $SrTiO_3$ single crystals. *Appl. Phys. Lett.* **78**, 3738–3740 (2001).
48. Rossel, C., Meijer, G. I., Brémaud, D. & Widner, D. Electrical current distribution across a metal-insulator-metal structure during bistable switching. *J. Appl. Phys.* **90**, 2892–2898 (2001).
49. Szot, K., Speier, W., Bilhmayer, G. & Waser, R. Switching the electrical resistance of individual dislocations in single-crystalline $SrTiO_3$. *Nature Mater.* **5**, 312–320 (2006).
50. di Vicenzo, D. P. Quantum computing and single-qubit measurements using the spin-filter effect. *J. Appl. Phys.* **85**, 4785–4787 (1999).

Acknowledgements

We thank M. Varela and E. Jacquet for their help in sample fabrication and N. D. Mathur, J. F. Scott and H. Kohlstedt for fruitful discussions. This study was partially supported by the Picasso France–Spain program, the CICYT of the Spanish Government Projects NAN2004-9094 and MAT2005-05656, FEDER, the E.U. Marie Curie mobility program, the project FEMMES of the French Agence National de la Recherche (ANR-05-1-45147), the European Science Foundation THIOX network and the E.U. STREPs Nanotemplates (Contract NMPA4-2004-505955) and MaCoMuFi (Contract FP6-NMP3-CT-2006-033221).
Correspondence and requests for materials should be addressed to M.B.
Supplementary Information accompanies this paper on www.nature.com/naturematerials.

Competing financial interests

The authors declare no competing financial interests.